Optics and Lasers in Engineering 57 (2014) 6–12

Contents lists available at ScienceDirect

Optics and Lasers in Engineering

journal homepage: www.elsevier.com/locate/optlaseng

A simple calibration procedure for structured light system

Huafen Luo [a,b], Jing Xu [a,b,c,*], Nguyen Hoa Binh [b], Shuntao Liu [d], Chi Zhang [e], Ken Chen [b,c]

[a] State Key Laboratory of Tribology, Tsinghua University, Beijing 100084, China
[b] Department of Mechanical Engineering, Tsinghua University, Beijing 100084, China
[c] Key Lab of Precision/Ultra-precision Manufacturing Equipment and Control, Beijing 100084, China
[d] Aircraft Industrial (Group) Co. Ltd, Chengdu 610091, China
[e] Department of Electrical and Computer Engineering, Michigan State University, East Lansing, MI 48824, USA

ARTICLE INFO

Article history:
Received 13 August 2013
Received in revised form
2 January 2014
Accepted 9 January 2014
Available online 27 January 2014

Keywords:
Structured light
Calibration
3D reconstruction

ABSTRACT

The structured light system with a camera and a projector is widely used in various fields. However, the accurate calibration, which is crucial for a structured light system, is usually complicate and time-consuming, especially in the projector calibration stage. In addition, the calibration error of a projector is relatively bigger than a camera. Hence, a structured light system without the projector calibration can greatly reduce the system calibration error and simplify the calibration process. In this paper, a calibration method without projector calibration is proposed, in which the projector's line-of-sights serves as spatially vectors invariant to the environment. By introducing four reference planes and building look-up-tables for the camera-projector pixel correspondence, the 3D reconstruction of the system can be obtained without any projector's information. A series of experiments were performed to evaluate the proposed method, and it turned out that its accuracy is about 0.0925 mm.

1. Introduction

As a fast and economical measurement method, structured light technology is a focus of research today [1–6]. A structured light system usually consists of a camera and a projector, Fig. 1. A series of coded patterns emitted by the projector fall on the object, and then patterns deformed by the object are imaged by the camera. The pixel correspondence between the camera and projector images can be easily found by decoding the patterns, making the structured light system more convenient to use compared with the stereo vision technology [7–9]. Therefore, the structured light technique is increasingly used in many fields [10–13].

A structured light system must be calibrated before performing the measurements. The calibration is crucial as it evaluates the system parameters which are necessary to infer 3D information from 2D images acquired by the camera [14]. The structured light system calibration has been the subject of a number of works over the years, and many calibration methods have been proposed. In this paper, existing calibration methods are divided into three categories: photogrammetry based on matrix transformation, triangulation and polynomial.

1.1. Photogrammetry based on matrix transformation

The pinhole model is adopted to describe the camera and the projector – two essential elements in the structured light system. Camera calibration has been studied extensively, and is relatively mature [15–18]. However, as the projector is not an information receiver, its calibration is more difficult than that of the camera, so the projector calibration has been the focus of a number of researches. To accomplish that, some literatures treated the projector as a kind of special (pseudo or inverse) camera, so that camera calibration methods can be applied in projector calibration; others, instead of solving the projector's parameters explicitly, paid attention to the patterns emitted by the projector and tried to estimate equations of light stripe planes.

1.1.1. Inverse camera

Generally, a camera can be seen as an operator which transforms a certain 3D "input" (an object) to a 2D "output" (an image). By employing an object with known dimensions, the "input" and "output" are all known, then the operator can be determined. It is totally contrary for the projector as it can not receive any information from the environment, i.e., its "input" is the 2D image. So many researchers choose to fix the projector image dimensions and try to solve the corresponding 3D coordinates. Falco et al. [19] and Cui et al. [20] projected a reference pattern with known dimensions to the calibration artifact in different poses and calculated the 3D correspondences with the aid of the calibrated

* Corresponding author at: State Key Laboratory of Tribology, Tsinghua University, Beijing 100084, China.
E-mail address: jingxu@tsinghua.edu.cn (J. Xu).

0143-8166/$ - see front matter © 2014 Elsevier Ltd. All rights reserved.
http://dx.doi.org/10.1016/j.optlaseng.2014.01.010

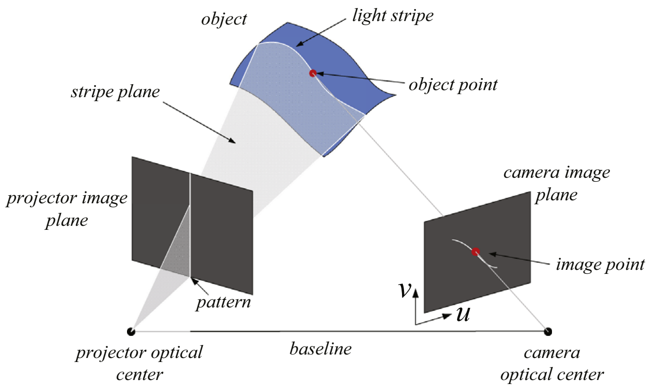

Fig. 1. Structured light system.

camera. Then the projector's parameters were determined in the same way as the camera. The main drawback of these approaches is the coupling of projector's and camera's calibration errors.

1.1.2. Pseudo-camera

To cope with the coupling of errors, some approaches tried to translate images captured by the camera into virtual images in the projector by finding the relation between camera's and projector's image planes, thus making the projector able to "see" the scene [21–25]. Literatures [21–23] built a correspondence map between projector pixels and camera pixels using the absolute phase algorithm, so for each camera image, a virtual projector image will be generated accordingly. Then with virtual images of the calibration target, the dimension of which is known, the projector's calibration can be done in the same way as the camera calibration. The main advantage of these approaches is that the projector and the camera are calibrated simultaneously, so the coupling of calibration errors is avoided. However, as the accuracy of the correspondence influences directly the projector calibration, there will no doubt be a propagation of the correspondence error.

1.1.3. Light stripes plane

In order to avoid the correspondence problem, many researchers proposed to calculate equations of light stripes planes directly. Literatures [26–28] tried to decide the light strips planes one-by-one with a series of control points. As the procedure should be repeated for every stripe, the overall time taken in such a system is considerable. Wei et al. [29] proposed to merely estimate equations of two planes, and derive other planes accordingly, simplifying the calibration process. Considering that the determination of 3D coordinates of the control points depends on camera parameters in all these approaches, there is an error propagation, too. Besides, these methods are only suitable for structured light system with line patterns.

1.2. Triangulation

The triangulation methods [30–32] focused on the triangular formed by camera's optical center O_c, projector's optical centre O_p, and the scene point P. They attempted to find the relationship between the height of scene point h, and several key parameters of the system such as the length of baseline O_cO_p, the height of the baseline, and the angle between camera's and projector's optical axis, and so on. In these approaches, the model is simpler than precedent methods, but the restriction on pattern direction and on the parallelism between O_cO_p and the reference plane, makes it difficult to implement the system.

1.3. Polynomial

Polynomial calibration (empirical calibration) approaches estimated the mathematical relationship between the phase ϕ and the height h by fitting a polynomial through N pairs of known phase and height for every pixel. Léandry et al. [33] and Liu et al. [34] proposed a polynomial model and an implicit conversion between the phase and the height, respectively. To get a high accuracy, the order of polynomial should be 4th or 5th, which means there are too many coefficients to calibrate. As the reference board should be moved precisely for every change of h, the calibration procedure is rather time-consuming. Simplifying the relationship to linearity [35,36], the number of coefficients can be reduced, but it suffers a low accuracy meanwhile. Anchini et al. [14] proposed a method in which just three poses of the reference board were needed, thus simplified the calibration process. However, it suffered a relatively low accuracy, too.

To sum up, there are three main drawbacks in existing calibration methods for structured light system: firstly, the dependence of the projector calibration on the camera calibration result or on the pixel correspondence, which leads to error propagation; secondly, the strict restriction in the system installation; slowness. Therefore, a fast, easy-to-operate and non-error-coupling calibration method needs to be found.

In this paper, a quite simple approach is proposed. We try to find the correspondence map between the camera image and the projector image pixel-by-pixel. Thus, for each pixel in the projector image, a series of corresponding pixels can be found in different images captured by the camera. By taking the projector's line-of-sights as spatially invariant vectors, the coordinates of a 3D point are expressed as a function of camera parameters and a series of pixel coordinates in the camera image plane. None of the projector's parameters need to be calibrated, thus the calibration procedure is rather simpler to operate. The measurement accuracy of a structured light system calibrated with this method is proved to be about ~0.0925 mm. The rest of the work is organized as follows. Section 2 describes the principle of the proposed calibration method in detail. Section 3 shows some experimental results. Finally, a brief conclusion is made in Section 4.

2. Calibration principle

2.1. Camera calibration

2.1.1. Camera model

The pinhole model, combined with lens distortion, is adopted to describe the camera in our work. According to the pinhole model, every projection line passes the camera's optical centre O_c, intersects with the image plane, and finally forms an image point, Fig. 2.

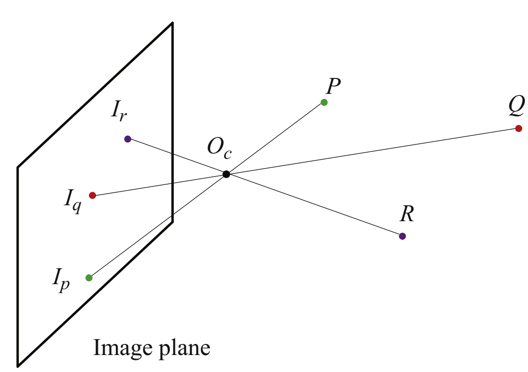

Fig. 2. Pinhole camera model.

The relationship between the 3D coordinates (x,y,z) of a scene point P and its image coordinates (u,v), given by point I_s, can be described as follows:

$$\lambda\begin{bmatrix} I_s \\ 1 \end{bmatrix} = K_c\begin{bmatrix} R_c & \overrightarrow{t_c} \end{bmatrix}\begin{bmatrix} P \\ 1 \end{bmatrix} \tag{1}$$

where λ is a scale factor;

$$K_c = \begin{bmatrix} \alpha & \gamma & u_0 \\ 0 & \beta & v_0 \\ 0 & 0 & 1 \end{bmatrix}$$

is the intrinsic matrix; (u_0, v_0) is coordinates of the principal point; α and β are the focal lengths along axes u and v, respectively; γ represents a skew parameter between axes u and v; $[R_c\ \overrightarrow{t_c}]$ is the extrinsic matrix with R_c the rotation matrix and $\overrightarrow{t_c}$ the translation vector.

The pinhole model is a first order approximation of the mapping from a 3D scene to a 2D image, so its validity, in general, decreases from the centre of the image to its edges because of the increasing lens distortion effects. A lens distortion model is introduced to compensate the geometric distortion caused by the optics. The relationship between the measured coordinates (u_d, v_d) and the ideal coordinates (u,v) of a given image point can be described as follows [37]:

$$\begin{cases} u_d &= (1+a_0r^2+a_1r^4+a_2r^6+a_3r^8+a_4r^{10})u \\ &\quad +(p_0+p_2r^2)(r^2+2u^2)+2(p_1+p_3r^2)uv \\ &\quad +s_0r^2+s_2r^4 \\ v_d &= (1+a_0r^2+a_1r^4+a_2r^6+a_3r^8+a_4r^{10})v \\ &\quad +(p_1+p_3r^2)(r^2+2v^2)+2(p_0+p_2r^2)uv \\ &\quad +s_1r^2+s_3r^4 \\ r^2 &= x^2+y^2 \end{cases} \tag{2}$$

where (a_0, a_1, a_2), (s_0, s_1) and (p_0, p_1) represent coefficients of radial, prism, and tangential distortion, respectively. The measured coordinates (u_d, v_d) of an image point should be firstly corrected according to Eq. (2), before employing Eq. (1).

2.1.2. Camera calibration

Camera calibration is to determine the intrinsic matrix, extrinsic matrix, and distortion coefficients. The calibration method developed by Vo et al.'s calibration approach [37] is applied in our approach. A flat board with printed ring patterns is used as the calibration target, Fig. 3. By analyzing images of calibration board in different poses, camera's parameters can be automatically estimated with the software Moiré, a software developed according to Vo et al.'s calibration approach. The calibration result of our camera is as below.

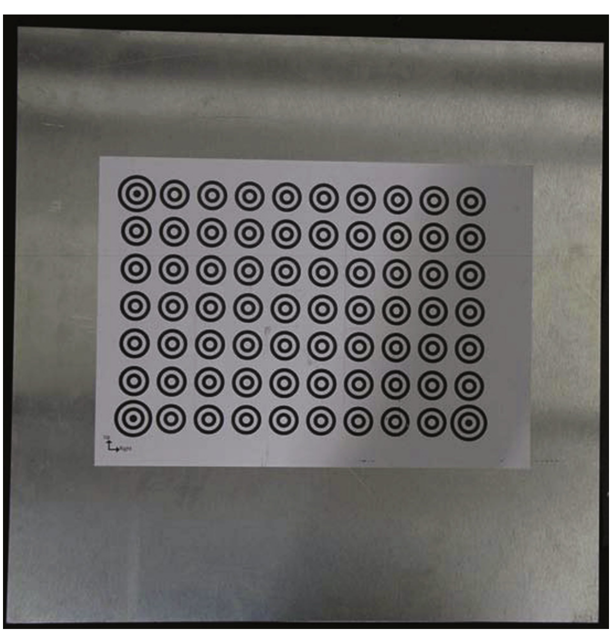

Fig. 3. Calibration board with ring patterns.

$$K_c = \begin{bmatrix} -2421.9508 & 0.1985 & 688.3313 \\ 0 & -2420.8673 & 503.9811 \\ 0 & 0 & 1 \end{bmatrix}$$

$$R_c = \begin{bmatrix} -0.9995 & -0.0090 & 0.0302 \\ -0.0090 & -1.0000 & 0.0000 \\ 0.0302 & -0.0002 & 0.9995 \end{bmatrix}$$

$\overrightarrow{t_c} = [103.1376\ \ 51.1850\ \ -931.9332]^T$
$a = [-0.0676\ \ 0.4016\ \ 1.1274\ \ -2.6890\ \ -0.4455]$
$p = [-0.0130\ \ 0.0015\ \ -0.0292\ \ 0.0044]$
$s = [0.0150\ \ -0.0009\ \ 0.0107\ \ -0.0051]$

2.2. 3D Reconstruction

The projector calibration is necessary in almost all the analytical calibration methods at present. However, as the projector is not an information-receiver, its calibration is complicated, and it causes a main error of the structured light system. To eliminate such an error, a calibration method avoiding the projector calibration is proposed in this paper. By taking every line-of-sight as a spatially invariant vector, we can obtain an additional constraint for the 3D reconstruction of a point with the information of two reference images. Combining it with two constraints from the camera, the 3D reconstruction can be built.

2.2.1. Equation of line-of-sight in the camera

For an arbitrary point, its Coordinates in the world frame $Oxyz$ can be transformed to coordinates in the camera system $O_cx_cy_cz_c$ by the following equation:

$$\begin{bmatrix} x_c \\ y_c \\ z_c \end{bmatrix} = R_c\begin{bmatrix} x \\ y \\ z \end{bmatrix} + \overrightarrow{t} \tag{3}$$

Applying Eq. (3) to the camera optical centre O_c, it comes to

$$0 = R_c\overrightarrow{O_c} + \overrightarrow{t} \tag{4}$$

with $\overrightarrow{O_c}$ the coordinates in the world frame of O_c. Then, obviously, we have

$$\overrightarrow{t} = -R_c\overrightarrow{O_c} \tag{5}$$

Combining Eq. (5) with Eq. (3), the relationship between the coordinates (x,y,z) of a 3D point P in the world frame, and the coordinates (u,v) of its correspondent image point I in the camera image plane can be expressed by

$$\lambda\begin{bmatrix} u \\ v \\ 1 \end{bmatrix} = K_cR_c\begin{bmatrix} I & -\overrightarrow{O_c} \end{bmatrix}\begin{bmatrix} x \\ y \\ z \\ 1 \end{bmatrix} \tag{6}$$

Then, we have

$$\lambda\begin{bmatrix} u \\ v \\ 1 \end{bmatrix} = K_cR_c(P-\overrightarrow{O_c}) \tag{7}$$

with λ is a scale factor. Set I' to be the homogeneous coordinates of I, i.e., $I' = (u,v,1)^T$. As K_c and R_c are invertible, it can be derived

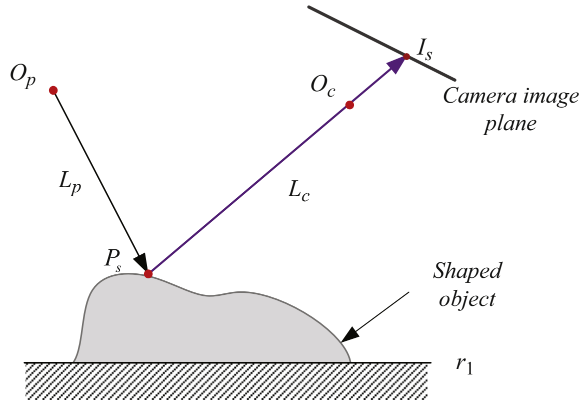

Fig. 4. 3D inspection of a shaped object.

from Eq. (4) that

$$P = \overrightarrow{O_c} + \lambda(K_cR_c)^{-1}I' \tag{8}$$

If we take λ as arbitrary, what Eq. (8) describes becomes not a point but a line, the line-of-sight L_c, to be exactly. Then we have

$$L_c = \overrightarrow{O_c} + \lambda(K_cR_c)^{-1}I' \tag{9}$$

as the equation of line-of-sight L_c.

2.2.2. Constraints from camera calibration

The 3D inspection process by a structured light system is illustrated in Fig. 4. A line-of-sight L_p, emitted by the projector from a given point I_p in the image plane, passes through the optical centre O_p, and is reflected to a line-of-sight L_c by point P_s on the object surface. Then L_c passes through O_c, the camera optical centre, and finally arrives at an image point I_s in the camera image plane. The world coordinate system $Oxyz$ is set up with planes Oxy coinciding with the reference plane r_1.

According to Eq. (9), once the camera is calibrated, the equation of line-of-sight L_c corresponding to I_s is

$$L_c = \overrightarrow{O_c} + \lambda(K_cR_c)^{-1}I'_s \tag{10}$$

with I'_s being the homogeneous coordinates of I_s, i.e., $I'_s = (u_s, v_s, 1)^T$. Let the scale factor corresponding to P_s be λ_s, then:

$$P_s = \overrightarrow{O_c} + \lambda_s(K_cR_c)^{-1}I'_s \tag{11}$$

Eq. (11) includes two constraints for the estimation of the 3D coordinates of P_s. If only one more constraint is found, the reconstruction problem will be solved. Therefore, we turn to the projector to get the constraint needed.

2.2.3. Projector constraint

As P_s falls also on line-of-sight L_p of the projector, it is collinear with arbitrary points on L_p. Therefore, by finding coordinates of two reference points which are on the same line-of-sight, an additional constraint can be obtained.

Two reference planes are used to generate reference point pairs, Fig. 5. r_1 and r_2 are parallel planes with a distance of h_0. L_p intersects r_1 at point $P_{r_1}(x_{r_1}, y_{r_1}, z_{r_1})$ and is reflected to the camera line-of-sight $L_c^{r_1}$. $I_{r_1}(u_{r_1}, v_{r_1})$ is the image point corresponding to P_{r_1}. Similarly, L_p intersects r_2 at point $P_{r_2}(x_{r_2}, y_{r_2}, z_{r_2})$ and finally forms an image point $I_{r_2}(u_{r_2}, v_{r_2})$ after being reflected into the camera by $L_c^{r_2}$. As P_{r_1}, P_{r_2} and P_s are collinear, we have $\overrightarrow{P_sP_{r_1}} \parallel \overrightarrow{P_{r_1}P_{r_2}}$, i.e.,

$$\exists \alpha \in \mathbb{R}, \quad \text{s.t. } \overrightarrow{P_sP_{r_1}} = \alpha\overrightarrow{P_{r_1}P_{r_2}} \tag{12}$$

Eq. (12) serves as the third constraint for the estimation of 3D coordinates of P_s.

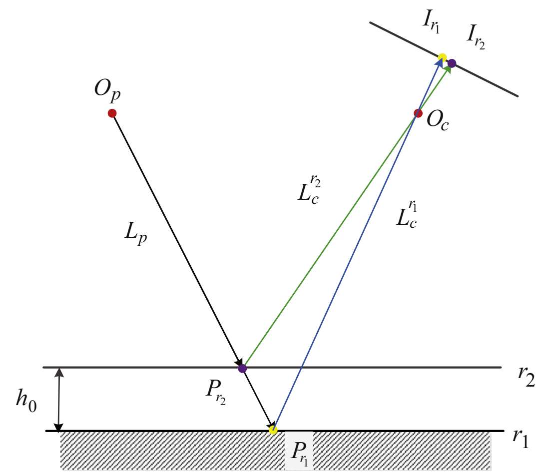

Fig. 5. Correspondence between two reference planes.

2.2.4. 3D reconstruction

The coordinates of P_{r_1} and P_{r_2} or their correspondent scale factors λ_{r_1}, λ_{r_2} should be determined before building the reconstruction of 3D point P_s. In the world frame $Oxyz$, equations of reference planes r_1 and r_2 are

$$r_1 : z = 0 \tag{13}$$

$$r_2 : z = h_0 \tag{14}$$

Similar to Eq. (10), $L_c^{r_1}$ and $L_c^{r_2}$ can be expressed by

$$L_c^{r_1} = \overrightarrow{O_c} + \lambda_1(K_cR_c)^{-1}I'_{r_1} \tag{15}$$

$$L_c^{r_2} = \overrightarrow{O_c} + \lambda_2(K_cR_c)^{-1}I'_{r_2} \tag{16}$$

where I'_{r_1} and I'_{r_2} are homogeneous coordinates of I_{r_1} and I_{r_2}, respectively; λ_1 and λ_2 are scale factors along $L_c^{r_1}$ and $L_c^{r_2}$. Use λ_{r_1} and λ_{r_2} to represent the scale factors corresponding to P_{r_1} and P_{r_2}, then we have

$$P_{r_1} = \overrightarrow{O_c} + \lambda_{r_1}(K_cR_c)^{-1}I'_{r_1} \tag{17}$$

$$P_{r_2} = \overrightarrow{O_c} + \lambda_{r_2}(K_cR_c)^{-1}I'_{r_2} \tag{18}$$

To facilitate the expression, a matrix $C = (K_cR_c)^{-1}$ is introduced. Then Eq. (17) can be written as

$$\begin{bmatrix} x_{r_1} \\ y_{r_1} \\ z_{r_1} \end{bmatrix} = \begin{bmatrix} x_{O_c} \\ y_{O_c} \\ z_{O_c} \end{bmatrix} + \lambda_{r_1}[C_1 \; C_2 \; C_3]^T \begin{bmatrix} u_{r_1} \\ v_{r_1} \\ 1 \end{bmatrix} \tag{19}$$

where C_i $(i=1,2,3)$ represents the ith row vector of C. The component of the coordinates of P_{r_1} along axis z is

$$z_{r_1} = z_{O_c} + \lambda_{r_1}C_3^T I'_{r_1} \tag{20}$$

Similarly,

$$z_{r_2} = z_{O_c} + \lambda_{r_2}C_3^T I'_{r_2} \tag{21}$$

λ_{r_1}, λ_{r_2} can be obtained by solving Eqs. (17), (18), (20) and (21).

$$\lambda_{r_1} = \frac{-z_{O_c}}{C_3^T I'_{r_1}} \tag{22}$$

$$\lambda_{r_2} = \frac{h_0 - z_{O_c}}{C_3^T I'_{r_2}} \tag{23}$$

Vectors $\overrightarrow{P_sP_{r_1}}$ and $\overrightarrow{P_{r_1}P_{r_2}}$ are determined by Eqs. (11), (17) and (18),

$$\begin{cases} \overrightarrow{P_sP_{r_1}} = (K_cR_c)^{-1}(\lambda_{r_1}I'_{r_1} - \lambda_s I'_s) \\ \overrightarrow{P_{r_1}P_{r_2}} = (K_cR_c)^{-1}(\lambda_{r_2}I'_{r_2} - \lambda_{r_1}I'_{r_1}) \end{cases} \tag{24}$$

Combining Eq. (12) we have

$$\lambda_{r_1}I'_{r_1} - \lambda_s I'_s = \alpha\left(\lambda_{r_2}I'_{r_2} - \lambda_{r_1}I'_{r_1}\right) \tag{25}$$

which can be written as

$$\begin{cases} \lambda_{r_1}u_{r_1} - \lambda_s u_s = \alpha(\lambda_{r_2}u_{r_2} - \lambda_{r_1}u_{r_1}) \\ \lambda_{r_1}v_{r_1} - \lambda_s v_s = \alpha(\lambda_{r_2}v_{r_2} - \lambda_{r_1}v_{r_1}) \end{cases} \tag{26}$$

By eliminating α, λ_s can be solved as

$$\lambda_s = \frac{\lambda_{r_1}\lambda_{r_2}(u_{r_1}v_{r_2} - u_{r_2}v_{r_1})}{\lambda_{r_2}(u_s v_{r_2} - u_{r_2}v_s) - \lambda_{r_1}(u_s v_{r_1} - u_{r_1}v_s)} \tag{27}$$

Substituting λ_s in Eq. (11), we have

$$P_s = \overrightarrow{O_c} + \frac{\lambda_{r_1}\lambda_{r_2}(u_{r_1}v_{r_2} - u_{r_2}v_{r_1})}{\lambda_{r_2}(u_s v_{r_2} - u_{r_2}v_s) - \lambda_{r_1}(u_s v_{r_1} - u_{r_1}v_s)}(K_cR_c)^{-1}I_s \tag{28}$$

Eqs. (22), (23) and (27) illustrate that the estimation of P_s only depends on I_{r_1}, I_{r_2}, I_s, h_0, and the camera parameters $\overrightarrow{O_c}$, K_c and R_c. Therefore, the reconstruction of the 3D point can be done without calibrating any of the projector parameters.

3. Experiments

3.1. System overview

In order to evaluate the proposed calibration method, two experiments were carried out with the structured light system in our lab, Fig. 6. The system is composed of a black and white CMOS camera (DH-HV1351UM) with a resolution of 1280×1024, and a projector (SONY VPL-EX70) with a resolution of 1024×768. The camera and the projector are fixed on two aluminium beams with their optical axis (not necessarily) almost parallel to each other. As the beams can be moved both horizontally and vertically, the distance between the camera and the projector, as well as their height relative to the ground, can be adjusted easily, making the system quite flexible. During the experiments, the camera and the projector is set up with a distance of 260 mm between each other, and the height of them is about 980 mm.

Graycode and line-shifting strategy [38] is adopted to code the projector patterns. To cover every pixel in the projector's image plane, 58 images are needed in total, with one full white, one full black, 30 vertical patterns (14 graycode patterns + 16 line-shifting patterns), and 26 horizontal patterns (15 graycode patterns + 12 line-shifting patterns). A flat board is employed for the camera calibration and for the reference data acquisition as well. To one side of the board, which is named as the calibration side, attaches printed ring patterns as shown in Fig. 3. The other side is painted white, and serves as the reference side.

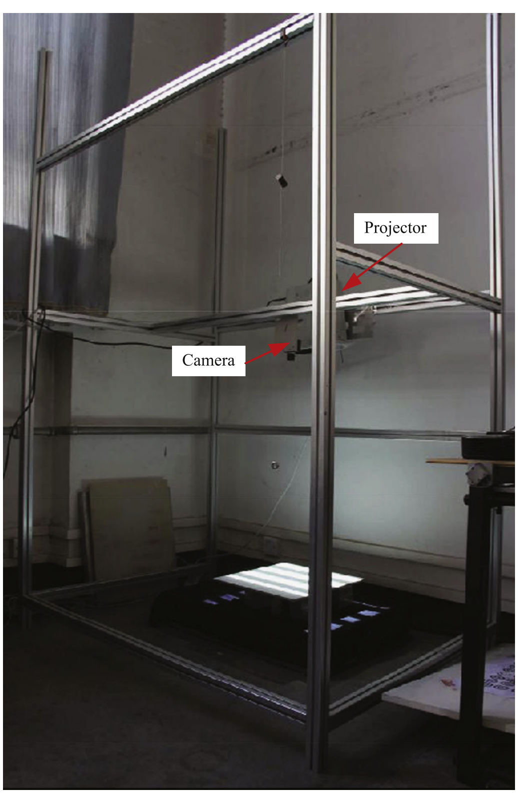

Fig. 6. The experimental setup.

3.2. Calibration and measurement procedure

The measurement procedure can be summarized as follows:

(i) Camera calibration: Set the calibration board in different poses and take a photo for each pose, so that 15–20 images can be acquired. Then the camera parameters can be obtained easily with the software Moiré. The calibration result is shown in Section 2.1.2. In the last pose, the board should be put on the ground (so it is almost horizontal) and it should be about in the centre of the camera's view field. Set up the world coordinate system $Oxyz$ so that its plane of Oxy coincides with the upwards surface of the board, i.e., its plane equation is $z=0$. Then turn over the plane board, so its reference side is upward and it serves as reference plane r_1 now.

(ii) Acquisition of the look-up table for r_1. Emit coded patterns to the reference plane and take a photo for each pattern. Decode the captured images to find the corresponding pixel in the projector to each camera pixel. Then, correct the camera pixels with the distortion coefficients obtained in step(i), and build the look-up table *LUT_ref*1, in which we can look up the corresponding camera pixel (u_{r_1}, v_{r_1}) for every projector pixel (i,j). The dimension of *LUT_ref*1 is $1024 \times 768 \times 2$.

(iii) Acquisition of the look-up table for r_{11}. Raise the board by 30 mm with some bricks, and now, the position of the reference side is called reference plane r_{11}. The plane equation of r_{11} is $z=30$. Calculate the look-up table *LUT_ref*11 for r_{11} by repeating step(ii).

(iv) Acquisition of the look-up table for r_{12} and r_2. Repeat step(iii) twice, so the look-up table *LUT_ref*12 and *LUT_ref*2 can be obtained. The plane equations of r_{12} and r_2 are $z=60$ and $z=90$ respectively. Then, remove the board and bricks.

(v) Acquisition of the look-up table of object to measure. Put the test object on the ground, and repeat step(ii), so we can get its look-up table *LUT_obj*, in which we can look up the corresponding camera pixel (u_s, v_s) for every projector pixel (i,j).

(vi) Re-correction of camera pixels in *LUT_ref*1, *LUT_ref*2 and *LUT_obj*. For each pixel of the projector, fit its corresponding camera pixels (u_{r_1}, v_{r_1}), $(u_{r_{11}}, v_{r_{11}})$, $(u_{r_{12}}, v_{r_{12}})$, (u_{r_2}, v_{r_2}) and (u_s, v_s) to a line named l. Find a point (u'_s, v'_s) in l so that the distance between (u_s, v_s) and (u'_s, v'_s) is minimum. Then replace (u_s, v_s) by (u'_s, v'_s) in *LUT_obj*. In the same way, correct the pixels (u_{r_1}, v_{r_1}) and (u_{r_2}, v_{r_2}) respectively.

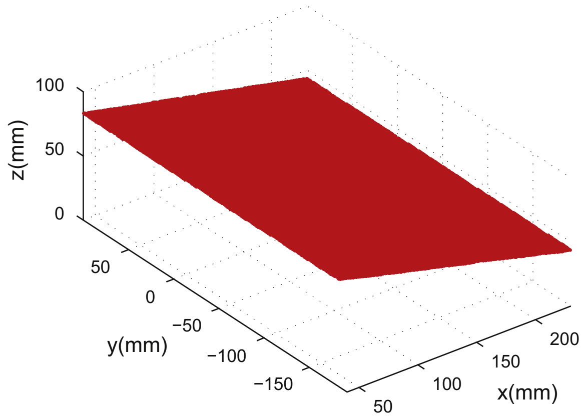

Fig. 7. 3D measurement result of a planar surface.

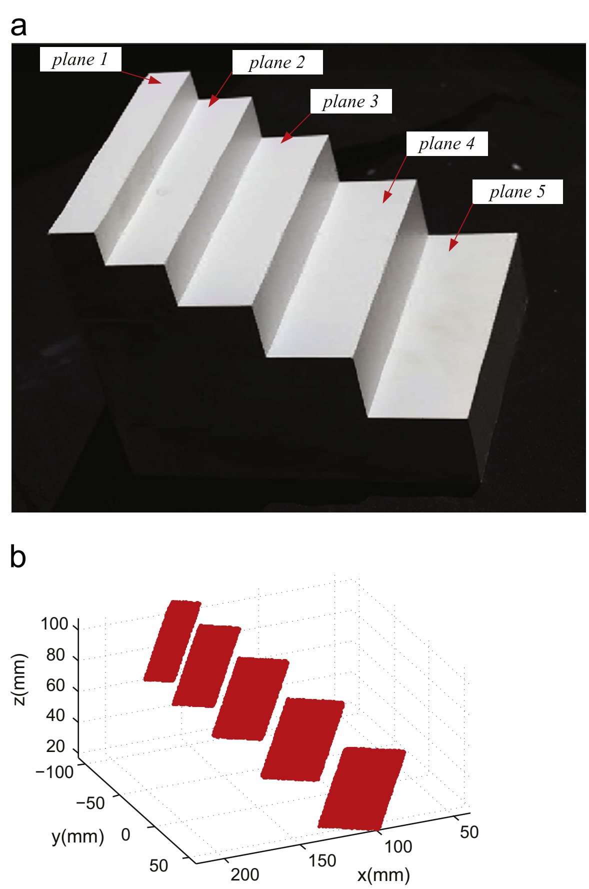

Fig. 8. 3D measurement result of a test brick: (a) test brick and (b) 3D reconstruction result.

(vii) 3D reconstruction of the object. Calculate the 3D point cloud using the principle mentioned in Section 2.

(Notice: For a certain system, the first four steps need to be performed only one time.)

3.3. *Experiment results*

Two experiments were performed. Firstly, a planar board with a white surface was measured. A point cloud was obtained following the procedure introduced in Section 3.2. Then, it was fitted to an ideal plane, and points with a distance greater than 0.5 mm from the ideal plane was taken as noise. The measurement result is shown in Fig. 7 with all noise removed. The density of the point cloud is greater than 420 cm^2. The distance of every point from the ideal plane was calculated. The standard Deviation is found to be about 0.0925 mm with a mean of 1.0826×10^{-4} mm, which shows that the proposed calibration method has a high accuracy.

Table 1
The measurement distance between planes.

Distance	Nominal value (mm)	Estimated value (mm)	Error with 4 refs (mm)	Error with 2 refs (mm)
d_{12}	15	14.9753	0.0247	0.0740
d_{23}	20	20.0315	0.0315	0.0205
d_{34}	25	25.0292	0.0292	0.0770
d_{45}	30	30.0344	0.0344	0.1029

Then, distance measurement was carried out. A brick with 5 stairs was chosen as the test object, Fig. 8(a). Only 5 planar surface were well exposed in the common field of view of the camera and projector because of its orientation, so the reconstruction result was composed of 5 point clouds. Fitting the point clouds to 5 ideal planes respectively and removing the noise, we got the measurement result as shown in Fig. 8(b). Distances between planes were calculated according to equations of the ideal planes.

The measurement result is given in Table 1, where $d_{ij}(i=1,\ldots,4;$ $j=2,\ldots,5)$ represents the distance between plane i and plane j. The second and third columns show that the measurement errors with 4 reference planes adapted in the calibration procedure. The maximum of the absolute error along axe z is found to be $\sim$0.034 mm. Then, the same measurement was carried out using 2 reference planes during the calibration and the corresponding errors are as shown in the last column in Table 1. Obviously, the measurement result with 4 reference planes is much better than that with only 2 reference planes. Therefore, the performance of the proposed approach can be improved with more reference planes adapted.

4. Conclusion

In this paper, a calibration of the structured light system has been proposed. By introducing four reference planes and building *LUTs* (look up tables) for the camera-projector pixel correspondence, the 3D reconstruction can be done without knowledge of any projector′s parameters. The avoidance of the projector calibration makes the calibration process faster, simpler, and more convenient to operate. Two experiments were performed with our structured light system. The results showed that the measurement accuracy achieved at $\sim$0.0925 mm. The calibration method proposed in this paper is tuned out effective and feasible.

Acknowledgments

This work is supported by Key Lab of Precision/Ultra-precision Manufacturing Equipment and Control of Beijing (Grand No. PMEC201205), National Natural Science Foundation of China (Grant No. 51105218), Research Fund for the Doctoral Program of Higher Education of China (Grant No. 20110002120053), and the Fund of State Key Laboratory of Tribology of China (Grant No. SKLT11C6).

References

[1] Hiroshi Kawasaki H, Furukawa R, Sagawa R, Yagi Y. Dynamic scene shape reconstruction using a single structured light pattern. In: IEEE conference on computer vision and pattern recognition. CVPR 2008. IEEE2008; 2008. p. 1–8.
[2] Chen S, Li Y, Zhang J. Vision processing for realtime 3-D data acquisition based on coded structured light. IEEE Trans Image Process 2008;17:167–76.
[3] Andrews DL. Structured light and its applications: an introduction to phase-structured beams and nanoscale optical forces. Academic Press; 2011.
[4] Scharstein D, Szeliski R. High-accuracy stereo depth maps using structured light. In: IEEE computer society conference on proceedings computer vision and pattern recognition, IEEE2003, vol. 191; 2003. p. I-195–I-202.
[5] Fofi D, Sliwa T, Voisin Y. A comparative survey on invisible structured light. In: Proceedings of SPIE2004. p. 90–8.
[6] Salvi J, Fernandez S, Pribanic T, Llado X. A state of the art in structured light patterns for surface profilometry. Pattern Recognit 2010;43:2666–80.
[7] Hussmann S, Ringbeck T, Hagebeuker B. A performance review of 3D TOF vision systems in comparison to stereo vision systems. Stereo Vis 2008: 103–20.
[8] M. Agrawal, K. Konolige, Real-time localization in outdoor environments using stereo vision and inexpensive GPS. In: 18th international conference on pattern recognition, ICPR 2006, IEEE2006. 2006. p. 1063–68.
[9] Koninckx TP, Van Gool L. Real-time range acquisition by adaptive structured light. IEEE Trans Pattern Anal Mach Intell 2006;28:432–45.
[10] Shotton J, Sharp T, Kipman A, Fitzgibbon A, Finocchio M, Blake A, et al. Real-time human pose recognition in parts from single depth images. Commun ACM 2013;56:116–24.
[11] McPherron SP, Gernat T, Hublin J-J. Structured light scanning for high-resolution documentation of *in situ* archaeological finds. J Archaeol Sci 2009;36:19–24.
[12] Zexiao X, Jianguo W, Qiumei Z. Complete 3D measurement in reverse engineering using a multi-probe system. Int J Mach Tools Manuf 2005;45: 1474–86.
[13] Jun Y. A piecewise hole filling algorithm in reverse engineering. Comput Aided Des 2005;37:263–70.
[14] Anchini R, Di Leo G, Liguori C, Paolillo A. A new calibration procedure for 3-D shape measurement system based on phase-shifting projected fringe profilometry. IEEE Trans Instrum Meas 2009;58:1291–8.
[15] Kannala J, Brandt SS. A generic camera model and calibration method for conventional, wide-angle, and fish-eye lenses. IEEE Trans Pattern Anal Mach Intell 2006;28:1335–40.
[16] Kim J-S, Gurdjos P, Kweon I-S. Geometric and algebraic constraints of projected concentric circles and their applications to camera calibration. IEEE Trans Pattern Anal Mach Intell 2005;27:637–42.
[17] Zhang Z. Camera calibration with one-dimensional objects. IEEE Trans Pattern Anal Mach Intell 2004;26:892–9.
[18] Zhang Z. A flexible new technique for camera calibration. IEEE Trans Pattern Anal Mach Intell 2000;22:1330–4.
[19] Falcao G, Hurtos N, Massich J. Plane-based calibration of a projector-camera system. VIBOT Master 2008;9.
[20] Cui H, Dai N, Yuan T, Cheng X, Liao W, Calibration algorithm for structured light 3d vision measuring system. In: CISP'08. Congress on image and signal processing, IEEE2008; 2008. p. 324–8.
[21] Chen X, Xi J, Jin Y, Sun J. Accurate calibration for a camera projector measurement system based on structured light projection. Opt Lasers Eng 2009;47:310–9.
[22] Li Z, Shi Y, Wang C, Wang Y. Accurate calibration method for a structured light system. Opt Eng 2008;47 053604-053604-053609.
[23] Zhang S, Huang PS. Novel method for structured light systemcalibration. Opt Eng 2006;45(083601):1–8.
[24] Gao W, Wang L, Hu Z. Flexible method for structured light system calibration. Opt Eng 2008;47 083602-083602-083610.
[25] Gao W, Wang L, Hu Z-Y. Flexible calibration of a portable structured light system through surface plane. Acta Automat Sin 2008;34:1358–62.
[26] Huynh D, Owens R, Hartmann P. Calibrating a structured light stripe system: a novel approach. Int J Comput Vis 1999;33:73–86.
[27] Zhou F, Zhang G. Complete calibration of a structured light stripe vision sensor through planar target of unknown orientations. Image Vis Comput 2005;23:59–67.
[28] Wei Z, Cao L, Zhang G. A novel 1D target-based calibration method with unknown orientation for structured light vision sensor. Opt Laser Technol 2010;42:570–4.
[29] Wei Z, Li J, Ji X, Bo Y. A calibration method based on multi-linear structured light. Procedia Eng 2010;7:345–51.
[30] Jia X, Zhang Z, Cao F, Zeng D. Model and error analysis for coded structured light measurement system. Opt Eng 2010;49(123603):1–9.
[31] Zhang Z, Zhang D, Peng X. Performance analysis of a 3D full-field sensor based on fringe projection. Opt Lasers Eng 2004;42:341–53.
[32] Sansoni G, Carocci M, Rodella R. Calibration and performance evaluation of a 3-D imaging sensor based on the projection of structured light. IEEE Trans Instrum Meas 2000;49:628–36.
[33] Leandry I, Breque C, Valle V. Calibration of a structured-light projection system: development to large dimension objects. Opt Lasers Eng 2012;50: 373–9.
[34] Liu H, Su W-H, Reichard K, Yin S. Calibration-based phase-shifting projected fringe profilometry for accurate absolute 3D surface profile measurement. Opt Commun 2003;216:65–80.
[35] Tao L, Harding K, Jia M, Song G. Calibration and image enhancement algorithm of portable structured light 3D gauge system for improving accuracy, Photonics Asia 2010, International Society for Optics and Photonics 2010, p. 78550Y-78550Y-78558.
[36] Tavares PJ, Vaz MA. Linear calibration procedure for the phase-to-height relationship in phase measurement profilometry. Opt Commun 2007;274: 307–14.
[37] Vo M, Wang Z, Luu L, Ma J. Advanced geometric camera calibration for machine vision. Opt Eng 2011;50(110503):1–3.
[38] Ghring J. Dense 3D surface acquisition by structured light using off-the-shelf components, photonics west 2001-electronic imaging. International Society for Optics and Photonic; 2000. p. 220–31.